Historical aerial photographs for landslide assessment: two case histories

J. Walstra, N. Dixon and J.H. Chandler

Quarterly Journal of Engineering Geology and Hydrogeology 2007; v. 40; p. 315-332
doi:10.1144/1470-9236/07-011

Historical aerial photographs for landslide assessment: two case histories

J. Walstra[1], N. Dixon[2] & J.H. Chandler[2]

[1]Department of Languages & Cultures of the Near East & North Africa, Ghent University, Sint-Pietersplein 6, B-9000 Ghent, Belgium (e-mail: Jan.Walstra@UGent.be)

[2]Department of Civil and Building Engineering, Loughborough University, Loughborough LE11 3TU, UK

Abstract

This paper demonstrates the value of historical aerial photographs for assessing long-term landslide evolution. The study focused on two case histories, the Mam Tor and East Pentwyn landslides. In both case histories we explored the variety of data that could be derived relatively easily using an ordinary PC desktop, commercially available software and commonly available photographic material. The techniques to unlock qualitative and quantitative data captured in the photographic archive were based on the principles of aerial photo-interpretation and photogrammetry. The products created comprised geomorphological maps, automatically derived digital elevation models (DEMs), displacement vectors and animations. The measured horizontal displacements of the Mam Tor landslide ranged from 0.09 to 0.74 m a^{-1} between 1953 and 1999, which was verified by independent survey data. Moreover, the observed displacement patterns were consistent with photo-interpreted geomorphological information. The photogrammetric measurements from the East Pentwyn landslide (horizontal displacements up to 6 m a^{-1} between 1971 and 1973) also showed a striking resemblance to independent data. In both case histories, the vertical accuracy was insufficient for detecting significant elevation changes. Nevertheless, DEMs proved to be a powerful tool for visualization. Overall, the results in this study validated the techniques used and strongly encourage the use of historical photographic material in landslide studies.

Landslides include a range of slope movements, representing a widespread geological hazard. Yearly, extreme landslide disasters worldwide pose threats to people and infrastructure, and cause significant economic losses. Growth of urban areas and expanded land use have increased the vulnerability of societies to landslides (Boullé *et al*. 1997; Smyth & Royle 2000). Moreover, the impact of climate change may result in higher frequencies of such events in the future (Dehn *et al*. 2000; Dixon & Brook 2007). Past research has identified different landslide mechanisms and many controls on their initiation and development (e.g. Varnes 1978; Crozier 1986). These controls are very complex and relate to climatic variables and characteristics of the slope, such as material, geological and hydrological conditions and vegetation cover. A full understanding of their interrelationships requires detailed and extensive monitoring of environmental factors and associated landform changes. Usually, long climate data records are available, whereas obtaining accurate historical spatial data quantifying landform change is a rather more challenging task.

A combination of multi-temporal mapping of surface features and monitoring of landslide displacements may result in better understanding of their underlying mechanisms. There are sophisticated tools available for monitoring landslide movements. Traditional instruments include inclinometers, tiltmeters, extensometers and land surveying devices (Franklin 1984). Modern tools include global positioning systems (GPS) (Gili *et al*. 2000; Mora *et al*. 2003; Mills *et al*. 2005; Squarzoni *et al*. 2005) and remote sensing techniques such as satellite images (Hervás *et al*. 2003; Delacourt *et al*. 2004), synthetic aperture radar (SAR) (Buckley *et al*. 2002; Squarzoni *et al*. 2003; Tarchi *et al*. 2003), and light detection and ranging (LIDAR) (Adams & Chandler 2002; Mills *et al*. 2005). The data record lengths of these techniques are restricted. Field techniques can provide only real-time data (unless the site has already been subject to monitoring in the past), and most modern techniques reveal only contemporary data. Satellite data are capable of dating back to the 1960s or 1970s, and aerial photographs potentially offer the most extensive data coverage, as systematic aerial surveys in the UK started after the Second World War (i.e. post-1945).

Indeed, aerial photographs are an accepted resource in landslide studies (e.g. Soeters & Van Westen 1996; British Standards Institution 1999). They not only provide a metric model from which quantitative measurements can be obtained, but also give a qualitative description of the Earth's surface. A sequence of photographs captures morphological change, which can be unlocked by using appropriate photogrammetric methods. Recent advances in information technology have led to the development of automated digital photogrammetric techniques, allowing for rapid and cost-effective data collection (Chandler 1999; Baily *et al*. 2003). Hence, the aerial photographic archive offers great potential for studying landslide evolution.

The aim of this paper is to demonstrate the value of historical aerial photographs for landslide assessment. The paper details key stages of such a study and uses two case histories to demonstrate the wide range of data

 1470-9236/07 $15.00

that can be extracted using modern digital photogrammetric techniques. Not only is the performance of automated techniques on archival images evaluated but also the relevance of the different products to landslide studies is indicated.

Methods

Theoretical principles

Techniques to unlock the data captured in aerial photographs are based on two main principles: aerial photo-interpretation (API) for qualitative analysis and photogrammetry for extracting quantitative spatial data.

Aerial photo-interpretation Photo-interpretation involves the systematic examination of photographic images for the purpose of identifying objects and judging their significance (Colwell 1960). The value of API for analysing slope stability has been widely acknowledged (e.g. Rib & Liang 1978; Brunsden & Prior 1984; Soeters & Van Westen 1996). Recognition of landslides is based mainly on the characteristic morphology, vegetation and drainage conditions of hill slopes (Soeters & Van Westen 1996). Diagnostic surface features can be related to certain types of movement, the degree of activity and depth of movement (Mantovani *et al*. 1996; Parise 2003). Repetitive mapping from photographs shows the progressive evolution of landslides and may lead to better understanding of their causal processes (Chandler & Cooper 1989; Chandler & Moore 1989; Chandler & Brunsden 1995; Van Westen & Getahun 2003).

A useful tool in presenting photo-interpreted information is geomorphological maps. They are used to convey information about the form, origin, age and distribution of landforms and their formative processes (Anon 1972; Brunsden *et al.* 1975). In addition, they reveal associations of landforms, which are essential for understanding both individual landforms and landscapes (De Graaff *et al.* 1987).

Photogrammetry Theoretical principles underlying photogrammetry were established over a century ago and further developed for map production in the 1930s (Slama 1980; Wolf & Dewitt 2000). The main concept of photogrammetry is collinearity, whereby an object point, the projection centre of a lens, and its corresponding image point on the focal plane lie along a straight line (Fig. 1). Using this principle, 3D coordinates can be extracted from any stereopair of photographs, provided that the inner geometry (interior orientation) and the position and orientation of the camera at the moment of exposure (exterior orientation) are known. However, a bundle of light rays will never pass from the object through the camera lens system and onto the imaging

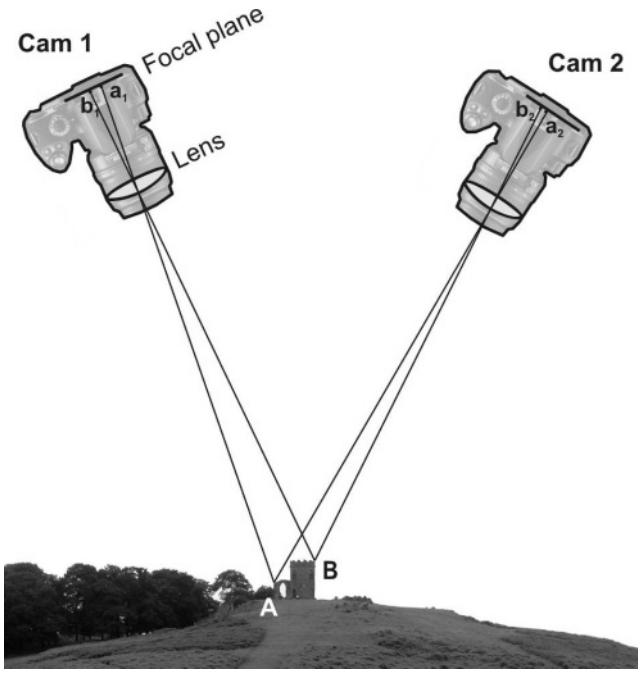

Fig. 1. The principles of photogrammetry: bundles of light rays pass from object points (A and B) through the perspective centre of the camera lens onto their corresponding image points (a and b) in the focal plane. Using two photographs from different camera positions (Cam 1 and Cam 2), 3D object coordinates can be determined by intersecting the reconstructed bundles of light. Some important parameters required for this procedure are the principal point and focal length of the lens.

device in a perfectly straight line. Therefore, for accurate photogrammetric work corrections have to be made for lens distortion, atmospheric refraction and Earth curvature (Wolf & Dewitt 2000).

The internal geometry of a camera is defined by the elements of interior orientation, or camera constants. For aerial mapping cameras, calibration certificates are usually provided by the camera manufacturer and include the location of the principal point, focal length of the lens, photo coordinates of the fiducial marks, and measures of lens distortion. The focal length is the distance from the principal point to the perspective centre. The principal point is the point at which the lens axis intersects the focal plane. Realization of the principal point is assisted by the fiducial marks, which are superimposed on the image and have a known position relative to the principal point. When using scanned imagery, a transformation is needed to define the relation between image (pixel) and photo coordinates. An affine transformation is normally used and is also able to compensate for film shrinkage as a result of ageing (Wolf & Dewitt 2000). An affine transformation is composed of one or several rotation, scaling and translation factors.

Solution of the non-linear collinearity equations requires an iterative procedure. Generally, a least-squares

solution is adopted in which all photographs are simultaneously adjusted to the ground control in one single solution. The unknowns associated with a bundle adjustment are typically the exterior orientation parameters of all the photographs. The measured elements include photo and ground coordinates of the control points, weighted according to their assumed precision. Advantages of the procedure are the limited ground control required and the minimization and distribution of errors between all image frames. Recent developments, such as airborne GPS and inertial navigation systems, have led to the capability to directly measure the exterior parameters, and include these observations in the bundle adjustment (Wolf & Dewitt 2000). The procedure offers the flexibility of incorporating additional parameters for estimating unknown camera parameters and other systematic distortions, then known as a self-calibrating bundle adjustment (Brown 1956; Kenefick *et al*. 1972; Granshaw 1980; Chandler & Cooper 1989). The inclusion of a stochastic model allows measurements of differing quality to be combined in a rigorous way. The measurements are weighted according to their variances, which are subsequently propagated through the functional model, thereby providing estimates of the variances of the derived data (Cooper & Cross 1988). All of these aspects are of great importance when historical photographs are used, as such images rarely provide a complete and accurate photogrammetric model.

Once the mathematical relationship between the photographs and ground surface has been established, coordinates can be extracted from anywhere on the site, and used to create digital elevation models (DEMs) and orthophotos. A DEM is a 3D representation of the terrain surface (Weibel & Heller 1991). In an orthorectified photograph, image distortions caused by camera tilt and terrain relief are eliminated so that all ground features are displayed in their true ground position (Wolf & Dewitt 2000).

Since the 1990s, significant developments in digital photogrammetry have allowed automation of large parts of the photogrammetric processing (e.g. Schenk 1996). A fundamental principle in the automation of DEM extraction is image matching. Image matching involves the identification of conjugate points in the overlapping area of stereo-images, corresponding to an identical object feature. A commonly applied matching strategy is area-based cross-correlation, in which small image patches are compared according to their grey-level distribution. As a result, very high-resolution DEMs and orthophotos can be created relatively easily using modern software packages, and have become standard outputs of the photogrammetric workflow (Wolf & Dewitt 2000).

For an extensive treatment of the photogrammetric techniques reference can be made to various textbooks (e.g. Wolf & Dewitt 2000; Luhmann *et al*. 2007).

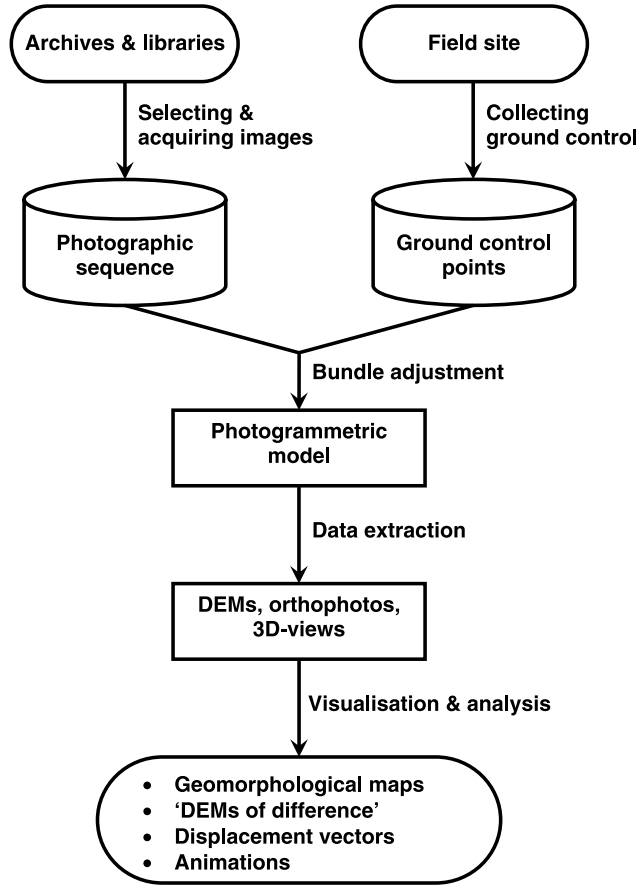

Fig. 2. Flowchart of the general working process adopted in this study.

Practical considerations

The working process adopted in this study can be divided in four general stages. First, suitable images were acquired. Then, ground control data were collected, using differential GPS. The next stage comprised the restitution of the photogrammetric model and data extraction. The final stage embraced visualization and analysis of the resulting data. This process is summarized in a flowchart (Fig. 2) and described in the following sections.

Stage 1: searching for suitable imagery Imagery is distributed among numerous archives and libraries in England and Wales, among them the National Monuments Record (English Heritage's public archive), Central Register of Air Photography for Wales, Ordnance Survey, the collection of Cambridge University, many commercial mapping companies and local authorities. Some of these institutions have standardized their search and request systems, whereby their archives can be searched online, but in some cases a visit to the archive is still required. For the case histories described here, selection of aerial photographs was based on the following considerations:

Fig. 3. Typical targets for ground control: the corner of an old barn and a gravestone.

(1) Ground coverage: it was ensured that the area of interest was completely covered by the stereoscopic overlap of two or more images.

(2) Time: sequential epochs were chosen, such that they were spanning a relevant time period.

(3) Scale: the scale of the photograph determined to what precision photo-coordinates could be measured and what features could be discerned.

(4) Geometry: the vertical precision was controlled by flying height, in relation to the airbase (ground distance between adjacent images) and the focal length of the lens.

(5) Image quality: sufficient radiometric contrast in the images was required to identify features and for a successful application of automated procedures.

(6) Format: best results were expected from using high-resolution scans (15–20 μm) of contact diapositives or original negatives, using a photogrammetric quality scanner; only when these were not available was the use of scans from contact prints considered.

(7) Camera calibration: calibration data were important for establishing an accurate photogrammetric model; if not available, the camera parameters had to be estimated through self-calibration.

Stage 2: collecting ground control Control points need to be identified and measured both on the photographs and on the ground surface. Such control points are required for establishing the photogrammetric model and referencing it to a ground coordinate system (i.e. defining the geometric datum). For the work described here control points consisted of physically well-defined features, easily accessible in the field and clearly identifiable on the photographs. An additional issue associated with historical photographs is that measured features need to be stable since the moment of image capture. Typical control points used included the corners of old buildings, stone walls and gravestones (Fig. 3). A minimum of two planimetric and three height points is needed to define a datum, but redundant control is desirable to increase the accuracy of the adjustment and for camera calibration. It also provides appropriate checks on data quality. In this study, the control points were distributed evenly over the area of interest to ensure strong geometry in the photogrammetric model.

The use of differential global positioning system (dGPS) is the recommended surveying technique for collecting ground control for photoscales of 1/4000–1/50 000 (Chandler 1999). High-precision geodetic GPS receivers were available for the practical work described here. Initially, a combination of Leica system 200 and 300 single-frequency receivers was used for surveying. Later, a set of two Leica system 500 dual-frequency receivers became available, allowing real-time processing via a radio link. In a 'stop-and-go' type of survey, one receiver was located at a fixed position (base station), and another (rover) was mounted on a pole and moved around the area of interest to record the positions of control points relative to the base station. The precision of this type of survey is typically 10–20 mm + 1 ppm horizontally and 20–30 mm + 1 ppm vertically (Uren & Price 2006), but depends on the observing conditions. An important control on precision is the number of satellites available and the geometry of their positions. It was therefore important to be aware of the changing satellite configuration throughout the day and the position of nearby mountains and buildings that might obstruct the satellite signals. For the principles of GPS surveying, reference can be made to standard textbooks (e.g. Leick 1990; Uren & Price 2006).

It was essential to reference the data to a global datum, to allow integration with other datasets. The UK National GPS Network allowed the positions to be referenced in ETRS89 coordinates. This network is established by the Ordnance Survey and consists of 50 active stations distributed over Great Britain (Ordnance Survey 2007). From the Ordnance Survey website, GPS data of a nearby active station were downloaded and used for data processing. The long continuous observation time of the base station (typically of the order of hours) allowed high-precision coordinates to be determined in relation to the active station. Post-processing

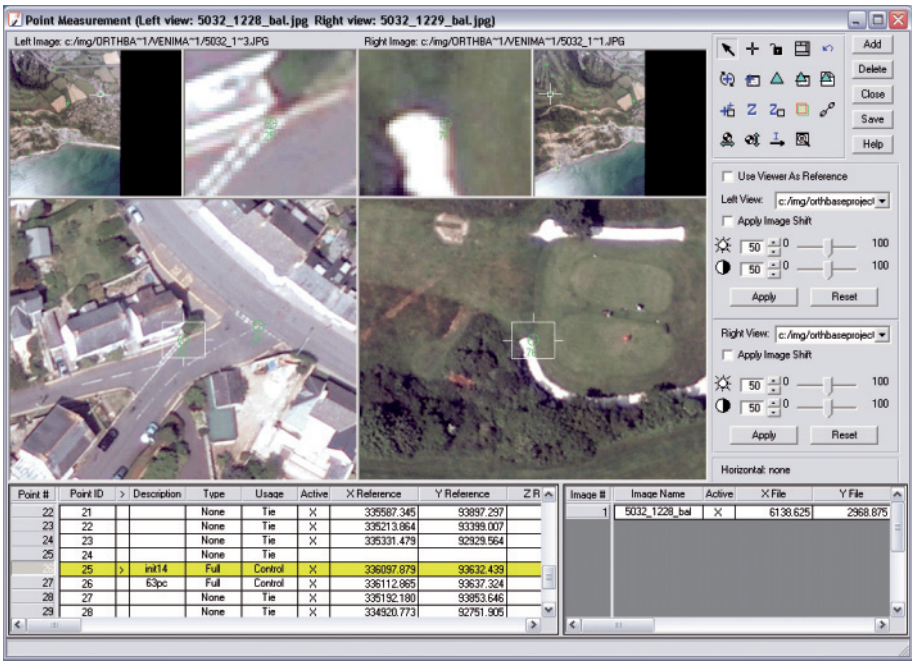

Fig. 4. Screenshot of the point measurement tool in LPS.

of the GPS data was performed by using Leica's SKI-Pro software (Version 2.5). The coordinates were transformed from ETRS89 to UK National Grid coordinates (OSGB36 datum) by using the online software provided by the Ordnance Survey, Grid InQuest (Version 6.0; Ordnance Survey 2007).

Stage 3: photogrammetric processing Photogrammetric software that operates on ordinary PC desktops is now widely available to perform all stages in the photogrammetric workflow (Fryer *et al*. 2007). A modest PC is capable of storing and manipulating the large datasets associated with digital imagery. Clear benefits of large computational power are the capability of solving large bundle adjustments through least-squares estimation and automation of the procedures. This automation is not only essential for generating extremely dense data, but also makes the techniques more accessible to non-photogrammetrists.

All of the work described in this paper was processed on a moderately equipped PC using Leica Photogrammetry Suite (LPS) software, version 9. LPS has a user-friendly interface guiding the user through the various steps of defining the interior orientation of the images, point measurement, bundle adjustment and eventually automated extraction of DEMs and orthophotos.

Ideally, the camera parameters were available from a camera calibration certificate and simply entered during the adjustment procedure. However, for some of the archival imagery these were missing and had to be estimated in the adjustment through self-calibration; in such cases, input of initial estimates of the parameters was required. Fiducial marks were identified on the images and used to define a 2D affine transformation between image and photo coordinates. Control points were identified and measured on the images in the graphical interface of the LPS point measurement tool, and their corresponding ground coordinates manually entered (Fig. 4).

All parameters and measurements were constrained in the adjustment by a stochastic model according to their assumed precision, specified through their standard deviation values. Once all data were entered, the bundle adjustment could be executed. To obtain a successful solution of such an iterative estimation procedure, it was important to have reasonable initial estimates of the unknown parameters. It was also helpful to increase redundancy of the measurements; for example, by adding tie points. These points, 'tying' frames together, were identified and measured on all the available images, without knowledge of their ground coordinates. LPS also allowed automatic tie point generation. Although strongly dependent on image quality, it was usually possible to create hundreds of extra measurements in this way. During this study the self-calibration procedures were performed by using the external program GAP (General Adjustment Program), developed by Clarke & Chandler (1992). In the latest version of LPS an option exists for including self-calibration in the bundle adjustment.

The primary products from the photogrammetric processing included DEMs and orthophotos. These were extracted using automated image matching techniques within the photogrammetric software and their quality was a function of the geometric accuracy of the photogrammetric model and the radiometric quality of the photographic images. To a limited extent, the results could be optimized in relation to the image characteris-

tics through adjustment of a number of user-defined parameters that affected the matching algorithm. The grid spacing of the DEMs was limited by the pixel dimensions, scale of the images and the size of the correlation window used during image matching. In addition to these automated techniques, the Leica software package also provided tools for stereo-viewing (StereoAnalyst) and creating virtual 3D views (VirtualGIS), allowing interactive measurement of object points.

Stage 4: data analysis These 'standard' products obtained from photogrammetry can be used for visualizing and analysing geomorphological change occurring on landslides in a number of different ways. In this study, the following uses of sequential images were evaluated: (1) geomorphological maps; (2) 'DEMs of difference'; (3) displacement vectors; (4) animations.

Sequential geomorphological maps were produced to show the progressive development and displacement of surface features. The primary aim was to identify different morphological elements in the landslide body that may correspond to specific movement styles. A qualitative interpretation of landslide processes is essential in the analysis of quantitative data (Mantovani *et al.* 1996; Parise 2003). Geomorphological boundaries were identified through 3D viewing of the photographs in StereoAnalyst. Then, the geomorphological features were mapped onto orthophotos to ensure geometric accuracy, and the possibility for quantitative comparison of maps obtained from different epochs. During a field survey the maps were checked and further details added.

A grid surface representing the change of form was created by subtracting two DEMs of different epochs from each other, using a simple graphical model in ERDAS Imagine. Such a surface of change, or 'DEM of difference', quantifies the effects of geomorphological processes. Areas experiencing removal of material will be indicated by depressions, whereas areas receiving material are indicated by peaks in the difference surface (Chandler & Cooper 1989).

Displacement vectors were obtained by measuring the position of identical features on different sets of photographs. Objects were interactively measured in a stereo-viewing tool (StereoAnalyst). Alternatively, these object points could be included as tie points in the bundle adjustment. The significance of displacements was assessed by evaluating measurements of stable objects. The spatial pattern of surface displacements provides information on the type of movement. Zones of lateral extension or compression coincide with areas that show respectively increasing and decreasing movement downslope (Baum *et al.* 1998). Also, the shape and depth of the slip surface can potentially be estimated based on surface displacements (Carter & Bentley 1985).

Sequential images were combined in animations to illustrate the progressive development of the terrain (Chandler *et al.* 2007). Image sequences, for example, consisted of orthophotos, 'DEMs of difference', or displacement fields. Animations were stored in universal formats such as animated GIFs or video files. 'Fly-through' animations, created by draping an orthophoto over a DEM, provided very realistic impressions of the sites.

Fig. 5. The Mam Tor landslide: head scarp on the right, debris slide on the left side, and the abandoned road crossing the central area. Inset: location of Mam Tor.

Case history 1: Mam Tor

This landslide (Fig. 5) is situated on the eastern flank of Mam Tor, just below the summit (517 m OD) at the head of Hope Valley in Derbyshire, UK (Ordnance Survey coordinates [SK135835]). The former main road between Sheffield and Manchester (A625) was constructed across the slide, but abandoned in 1979 as a consequence of continual damage caused by the moving ground mass. The initial rotational failure, in a slope consisting of sandstone sequences overlying shales, has been dated back to 3600 BP (Skempton *et al.* 1989). While advancing downhill, the mass broke into a complex series of blocks and slices, eventually creating a debris mass. The most active part moved 0.35 m a^{-1} on average over the last century (Rutter *et al.* 2003). There is evidence that present movements are not continuous but accelerate during wet winters, when rainfall exceeds certain limits (Waltham & Dixon 2000; Dixon & Brook 2007).

An important advantage in choosing this site was the availability of several information sources on surface displacements that have taken place over the last century. Notes about regular disturbances and road repairs, from 1907 until the final closure in 1979, have been recorded by the Derbyshire County Council. After closure of the road, repeated surveys and monitoring schemes have been set up by several universities: 1981–1983 by Sheffield University (Al-Dabbagh & Cripps 1987), 1990–1998 by Nottingham Trent University (Waltham & Dixon 2000) and since 1996 by Manchester University (Rutter *et al.* 2003).

Table 1. *Characteristics of the acquired photographic record of Mam Tor*

Date	Source	Scale	Focal length	Scan resolution (μm)	Ground resolution (m)	Image type	Format (cm)	Original medium
1953	NMR	1/10 700	20 inch (547 mm[1])	42	0.45	B/W vertical	18 × 21	Contact prints
1971	NMR	1/6400	304 mm[1]	42	0.27	B/W vertical	23 × 23	Contact prints
1973	CUCAP	1/4300	153 mm	15	0.065	B/W vertical	23 × 23	Diapositives
1973	CUCAP	Oblique	207 mm[1]	15	Variable	B/W oblique	12 × 13	Diapositives
1984	ADAS	1/27 200	152 mm	15	0.41	B/W vertical	23 × 23	Diapositives
1990	CUCAP	1/12 000	153 mm	15	0.18	B/W vertical	23 × 23	Diapositives
1995	CUCAP	1/16 400	152 mm	15	0.25	Colour vertical	23 × 23	Negatives
1999	Infoterra	1/12 200	153 mm	21	0.26	Colour vertical	23 × 23	Negatives

NMR, National Monuments Record; CUCAP, Cambridge University Collection of Aerial Photographs; ADAS, Agricultural Development and Advisory Service. B/W, black and white photographs.
[a]Estimated values from self-calibration.

Acquired photographs

A search for aerial photography of Mam Tor revealed a large number of images available from 1947 until the present. From a geomorphological point of view it was desirable to have an extensive sequence separated at regular intervals, to obtain a record of the development of the landslide. From a photogrammetric perspective it was of interest to acquire not only the best-quality photographs, but also a variety of formats, scale, media and quality. This provided an opportunity to investigate the application of the photogrammtric techniques to commonly available photographic archival material. A photographic sequence including eight epochs was composed, covering a period of almost half a century: 1953, 1971, 1973 (vertical and oblique images), 1984, 1990, 1995, 1999. Table 1 summarizes the characteristics of the acquired photographs; two typical examples of archival images are displayed in Figure 6.

A dGPS survey resulted in 27 control and check-points, processed to a precision of less than 0.01 m. Photogrammetric models for all epochs were adjusted in LPS. Because of the lack of camera parameters, these were estimated in a self-calibrating bundle adjustment for the 1953, 1971 and 1973 (oblique) photographs. For all other epochs, calibrated values were readily available from calibration certificates. The achieved accuracies of the solutions (Table 2) were largely dependent on the resolution of the images and the availability of calibration data. Consequently, the 1953 and 1971 photographs resulted in relatively poor data accuracy. Inherent to the geometry of standard aerial surveys, vertical accuracy was usually worse than horizontal. Important for the vertical accuracy was the base distance/height ratio of the images; relatively small base distances resulted in a weak geometry. The accuracy of DEMs derived from the oblique imagery was highly variable, and a function of the varying scale across the images.

Aerial photo-interpretations

Characteristic features of the landslide can be observed on the aerial photographs (Fig. 7), especially when viewed in three dimensions. The most striking feature of the landslide is the head scar with a height of 80 m in the Mam Tor sandstone beds (A); active rockfalls supply the colluvium below with fresh scree, which forms well-defined fans. Regressive failures have occurred in the southern part of the head scar and in the colluvium material (B). The upper part of the slide mass consists of largely intact blocks forming an irregular topography (C). At the front of this zone, individual blocks are breaking up, thereby developing large steps in the upper road section (D). This zone is bounded upslope by a scarp, marking the steeper inclined slip surface. The material from this cliff breaks up into a debris slide, extending further downhill. The plastic behaviour of the debris slide is demonstrated by the distortion of the lower road section, which is badly twisted and sheared. The debris slide lobe forms an undulating topography, which is badly drained, as indicated by the presence of several ponds and bracken (E). The presence of more developed vegetation cover along the southern margins suggests little movement in this part. The northern part of the toe is steeply inclined and its progression led to the destruction of Blacketlay Barn (F) (Waltham & Dixon 2000).

A detailed geomorphological map of the landslide area was created through photo-interpretation of the 1990 images (Fig. 8). The location of major geomorphological units remained unchanged during the entire image sequence (1953–2000), and therefore it was not justified to map these from the different epochs. Even so, this single geomorphological map proved to have great value for identifying the different elements in the landslide body and in helping to interpret the quantitative data that were extracted from the photographs in later stages.

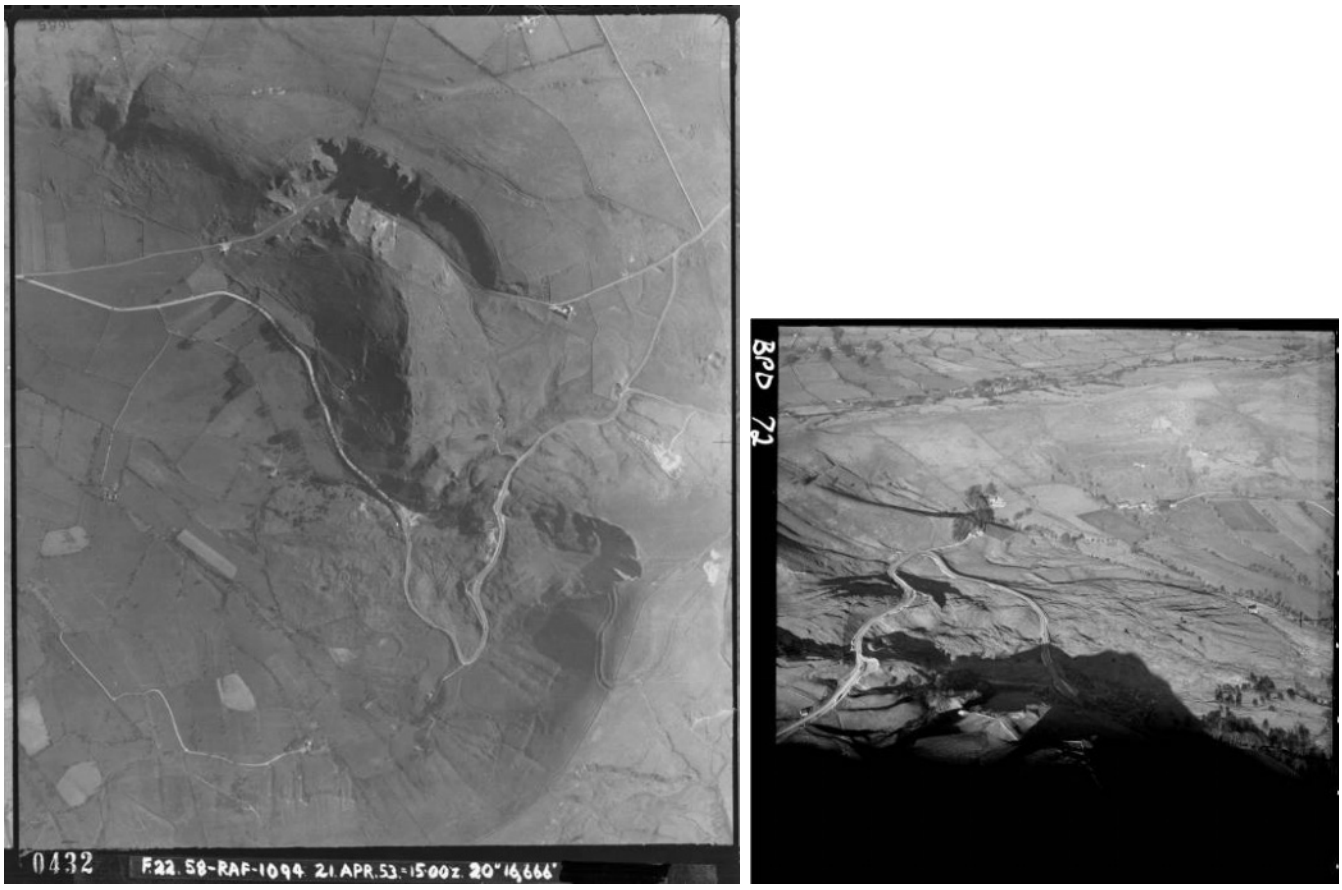

Fig. 6. Typical examples of archival photographs: the Mam Tor landslide on a vertical RAF image from 1953 (left) and the central part of the landslide as seen from the west on an oblique image from 1973 (right; Copyright reserved Cambridge University Collection of Air Photographs). These examples clearly illustrate that available material does not always have the ideal qualities for photogrammetric analysis. The RAF image was taken from great height and is hazy; in the oblique image large parts of the landslide are obscured by shadows.

Table 2. *Mam Tor: achieved accuracies of the photogrammetric solutions, DEMs and orthophotos, assessed by independent checkpoints*

Date	Ground resolution	Base/height ratio	Accuracy of photogrammetric model		Accuracy of DEM	Accuracy of orthophoto
	(m)		r.m.s.e. *xy* (m)	r.m.s.e. *z* (m)	SE *z* (m)	r.m.s.e. *xy* (m)
1953	0.45	1/8.0	1.50	4.21	5.22	1.65
1971	0.27	1/3.4	0.62	1.16	1.34	0.86
1973	0.065	1/2.5	0.31	0.54	0.76	0.88
1973 (obliques)	Variable	1/1.3–1/5.6	0.31	0.21	0.96/2.52	–
1984	0.41	1/1.7	0.60	1.67	1.58	1.38
1990	0.18	1/1.8	0.43	0.41	0.83	0.34
1995	0.25	1/1.9	0.42	0.47	0.76	0.69
1999	0.26	1/1.9	0.40	0.74	1.13	0.34

From the obliques only two pairs of photographs allowed DEM extraction (therefore two different values for DEM accuracy are given) and no orthophotos were created from this epoch.

All surface features clearly indicated a rotational type of movement in the upper part (arc-shaped scarp, transverse cracks dividing the upper body into several blocks, en echelon cracks along the sides, bulging at the foot) and a flow slide in the lower part (transverse pressure ridges, radial cracks and drainage pattern in lobe).

Digital elevation models

DEMs were automatically extracted from all eight image epochs. A grid spacing of 1 m was used, except for the 1953 and 1984 epochs, which required a larger cell size because of their lower ground resolution. The DEM

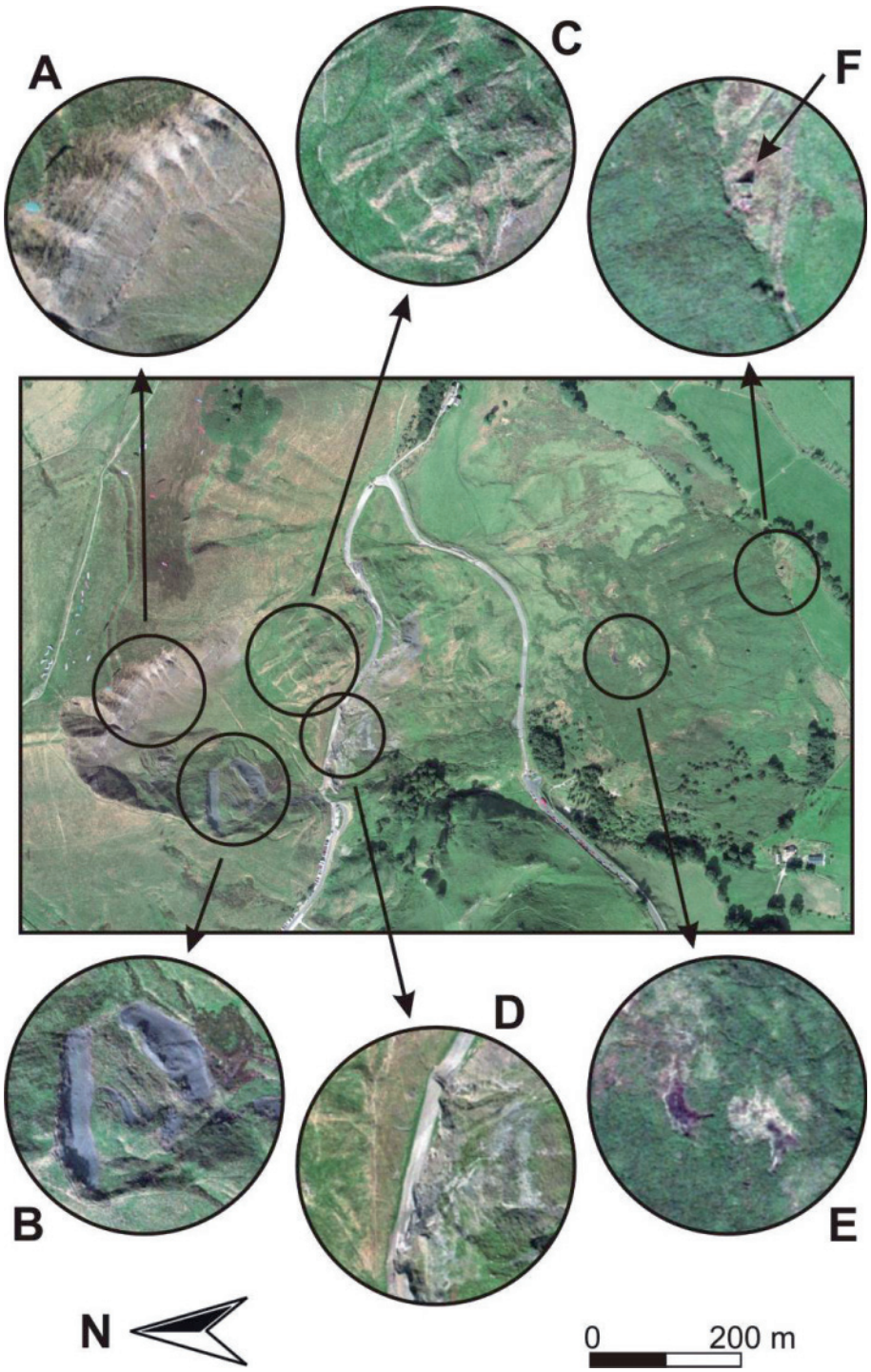

Fig. 7. Characteristic features of the Mam Tor landslide, visible on the 1999 images: A, head scar; B, regressive failure; C, irregular topography; D, destroyed road; E, ponds and bracken; F, Blacketlay Barn.

extraction parameters were optimized according to the guidelines provided by LPS (Leica Geosystems 2003). Especially in the case of poor-quality images (1953, 1971 and 1999 epochs), adjustments were made to improve the automated image matching between the photographs to overcome their poor image contrast. Checkpoints provided an indication for the accuracy of the extracted elevation models (Table 2).

Considering the relatively small vertical displacements of the landslide compared with the vertical data accuracy that was achieved, it was not possible to detect significant transportation of ground volumes. In spite of their limited quantitative value, the 'DEMs of difference' certainly demonstrated evidence of morphological change that is consistent with the geomorphological processes operating. Figure 9 shows a 'DEM of

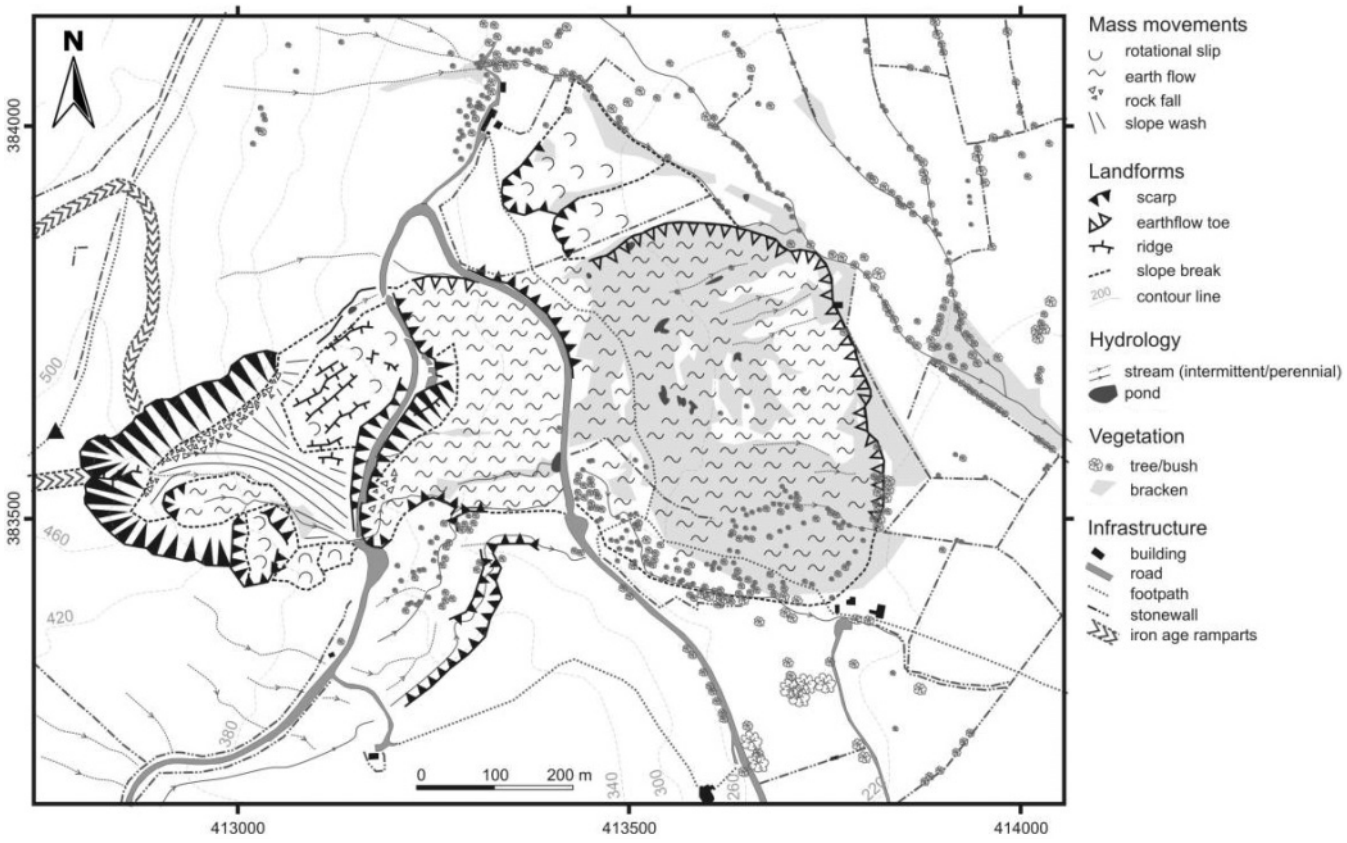

Fig. 8. A geomorphological map of the Mam Tor landslide, created through photo-interpretation of the 1990 images.

difference' of the central most active part of the landslide, obtained through subtracting the 1973 and 1999 DEMs. Of particular interest are the transverse pressure ridges, with positive height difference downslope and negative values upslope, which are consistent with downhill displacement.

Displacement vectors

As surface deformations of the landslide are rather slow, it was expected that surface features could easily be identified throughout the image sequence, and their displacements measured. A significant problem was that the terrain is largely covered with vegetation, and seasonal changes mask long-term changes of the ground surface. In the pre-1979 epochs, the road could not provide suitable targets, as its surface was constantly distorted and repaired. Eventually, a total of 50 features were identified in most of the epochs. These features included bushes and trees, ponds, stone walls, boulders, and (only in recent epochs) features on the road surface.

The displacements were visualized using vector plots, showing spatial variation in magnitude and orientation during a particular time interval. Figure 10 shows horizontal displacement vectors of the period 1973–1999. Vectors piercing the error ellipses represent significant displacements at a confidence level of 95%. Measurement of targets throughout the image sequence created a time series of displacements and showed the variation through time.

The observed horizontal movement pattern matches the morphological interpretation. The predominantly southeastern direction of the movements in the upper part of the slide suggests that the slip surface is largely controlled by the dip of the geological strata. In the lower part, the movement direction suggests that the slip surface is controlled by the original hill slope. At the toe, movements tend to be slightly outward directed, which implies an outward spreading of the flow slide. The large displacements in the upper part of the slip suggest a zone of extension, which corresponds to the observed transverse cracks in this area. Decreasing displacements below the lower road section coincide with the observed pressure ridges.

Averaged movement rates were compared with values obtained from previous ground surveys. Mean horizontal displacement of the landslide calculated from aerial photography between 1953 and 1999 was found to be *c.* 0.21 m a^{-1}, varying from *c.* 0.09 m a^{-1} at the toe to *c.* 0.74 m a^{-1} in the central part. These values are of comparable magnitude to the movement rates found by Rutter *et al.* (2003), 0.04–0.35 m a^{-1} over the last century and up to 0.50 m a^{-1} in recent years.

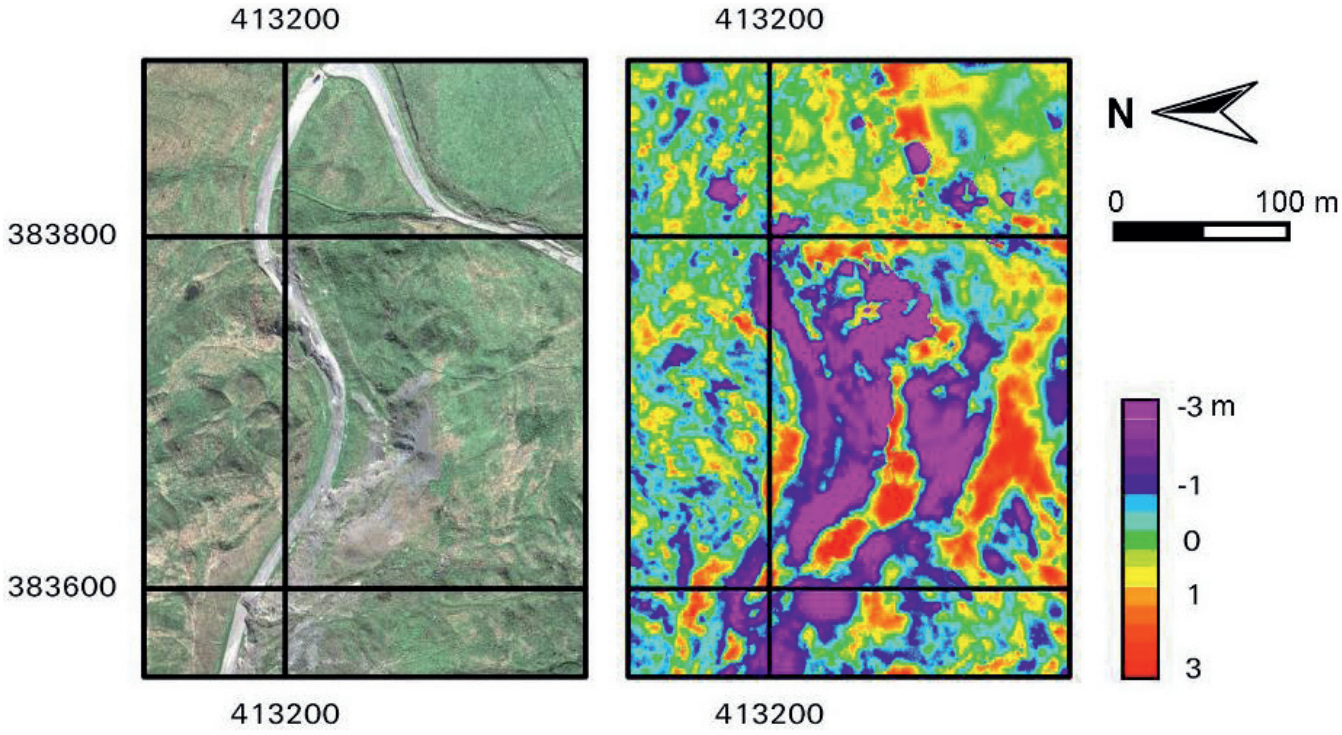

Fig. 9. A 'DEM of difference' of the central part of the Mam Tor landslide, obtained through subtracting DEMs from the 1973 and 1999 epochs.

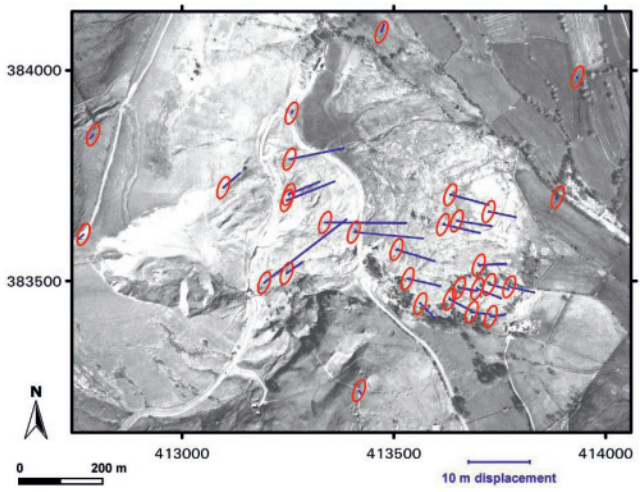

Fig. 10. Horizontal displacement vectors of the Mam Tor landslide, obtained through measurements from the 1973 and 1999 image epochs.

Animations

An animation created from orthophotos of the central part of the landslide, derived from the image sequence, allowed clear visualization of the progressive change of the surface (Fig. 11). In particular, the displacement and disintegration of the road is striking. Draping orthophotos over a DEM provided very realistic 3D views of the site, and these were used to produce fly-through animations (Fig. 12). The created animations are also available electronically (Walstra 2007).

Case history 2: East Pentwyn

The East Pentwyn landslide (Fig. 13) is situated on the eastern face of Ebbw Fach valley, south of Blaina, in the South Wales Coalfield (OS coordinates [SO207075]). The landslide is a typical example of the many deep-seated rotational failures in this region. These are typically associated with a combination of factors: steep valley sides, thick argillaceous strata and mining subsidence (Conway *et al.* 1980). The primary failure was triggered as recently as 1954. The displaced block disaggregated into a boulder field from which two debris slide lobes developed, advancing downhill. The debris slides eventually led to the abandonment of 12 houses (Siddle 2000). Remedial measures during the 1980s slowed down the continuing movements. Ground movements were monitored to quantify the effects of these works and observe further development of the slide (Jones & Siddle 1988).

Because of its young age, the complete development has been well documented and can be observed from historical aerial photographs. Records of monthly displacements are available for the period between 1982 and 1988 (Halcrow 1989). Throughout this period, movement rates were highest in the boulder field (up to 6 m a^{-1}) and showed a clear seasonal pattern (Halcrow 1983).

Acquired photographs

A search for aerial photography by the Central Register of Air Photography for Wales resulted in a large amount

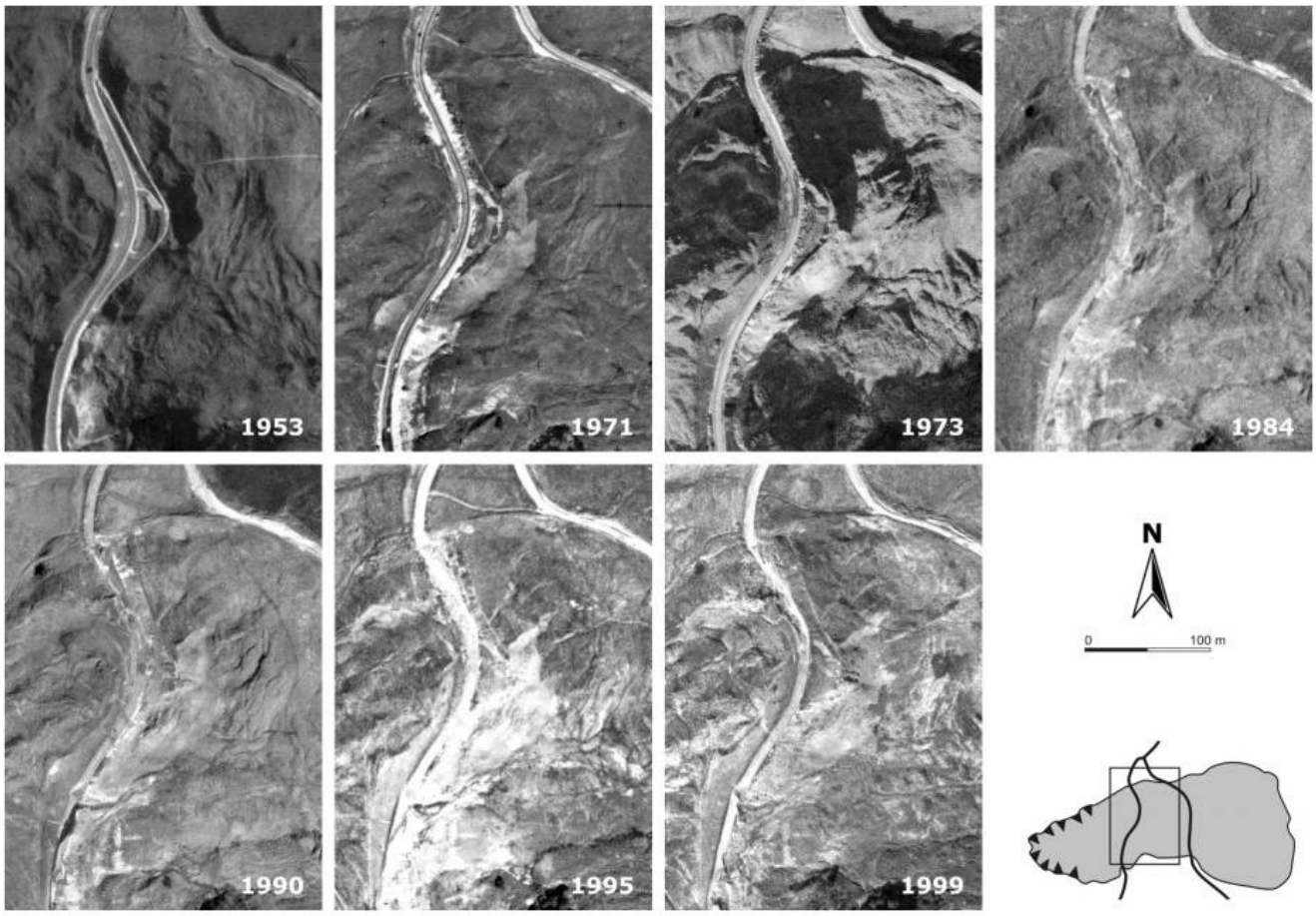

Fig. 11. An orthophoto sequence of the central part of the Mam Tor landslide.

Fig. 12. A realistic impression of the Mam Tor landslide, created through draping an orthophoto over a DEM, both obtained from the 1999 images.

Fig. 13. The East Pentwyn landslide: head scar visible at the back, the boulder field in the central part and the two vegetated debris slide lobes below. In the forefront is East Pentwyn farm. Inset: location of East Pentwyn.

of imagery covering the study area. Although the rather limited quality of old RAF photography was recognized, these photographs offered a unique opportunity to present images from close before and after the catastrophic failure. For this reason it was decided to acquire pairs of photographs from 1951 and 1955. In contrast, the image pairs from 1971 and 1973 were selected because of their good photo quality and similar illumination conditions. Assuming displacement rates comparable with those for the 1982–1983 period, displacements should be large enough to allow detection using these photographs. Photogrammetric-quality scans were obtained for all four epochs. Details of this photographic record are presented in Table 3.

Table 3. *Characteristics of the acquired photographic record of East Pentwyn*

Date	Source	Scale	Focal length	Scan resolution (μm)	Ground resolution (m)	Image type	Format (cm)	Original medium
1951	CRAPW	1/9800	20 inch (508 mm)	14	0.14	B/W vertical	18 × 21	Diapositives
1955	CRAPW	1/9200	20 inch (508 mm)	14	0.13	B/W vertical	18 × 21	Diapositives
1971	BKS Surveys	1/13 000	153 mm	14	0.18	B/W vertical	23 × 23	Diapositives
1973	CRAPW	1/8000	152 mm	16	0.13	B/W vertical	23 × 23	Diapositives

CRAPW, Central Register of Air Photography for Wales. B/W, black-and-white photographs.

Table 4. *East Pentwyn: achieved accuracies of the photogrammetric solutions, DEMs and orthophotos, assessed by independent checkpoints*

Epoch	Ground resolution	B/H ratio	Accuracy of photogrammetric model		Accuracy of DEM	Accuracy of orthophoto
	(m)		r.m.s.e. *xy* (m)	r.m.s.e. *z* (m)	SE *z* (m)	r.m.s.e. *xy* (m)
1951	0.14	1/6.8	1.96	8.03	7.91	1.93
1955	0.13	1/7.6	1.11	10.85	7.80	0.47
1971	0.18	1/1.9	0.26	0.58	1.75	1.45
1973	0.13	1/1.7	0.51	0.78	1.76	0.84

Ground control data were again collected using differential GPS. Because the valleys in this region have undergone major changes after mining activities ceased, it was sometimes difficult to find suitable ground control that could be identified throughout the 50 year period. However, ground coordinates of 59 control and checkpoints were recovered to a precision of 0.01 m.

Camera calibration data were available only for the 1971 dataset. A limitation of this epoch, however, was the presence of a high degree of radiometric noise, forming a 'salt and pepper' pattern, and hampering automatic image matching procedures. The noise was removed before processing was conducted, but this only assisted visualization. Tie point generation in significant parts of the images (especially the uphill areas) remained difficult because of low image contrast. Although the 1973 images were obviously captured with a metric camera, a calibration certificate was lacking. The clear fiducial marks allowed an accurate estimate of the principal point position. Values for focal length and flying height were displayed on the data strip of the frames. Because the radial distortion parameters could not be estimated adequately and were judged insignificant, these were ignored. The RAF imagery from 1951 and 1955 presented a real challenge: they were not only blurred and had a poor geometry, but also showed large systematic distortion, which could not be modelled. Therefore, an unsatisfactory camera model was used and low vertical accuracy had to be accepted. The achieved accuracies are summarized in Table 4.

Aerial photo-interpretations

In spite of their limited use for quantitative measurements, the 1951 and 1955 imagery offered a good opportunity for qualitative analysis. A sequence of orthophotos clearly shows the extent of the major failure that occurred in 1953 and subsequent movements (Fig. 14). On the 1951 photographs tension fissures are already visible at the position of the scarp later formed by the failure (A). In spite of the poor image quality, the failure is clearly visible on the 1955 photographs: debris lobes overrode and reactivated the old solifluction lobes (B), reaching all the way down to the houses of 'Henwaun Row' (D). The linear ridges across the lobes suggest a plastic type of movement. The upper part of the mass is covered with scree and boulders (C). Unfortunately, the main scarp is obscured by shadows. The 1973 orthophoto clearly shows that the slide is still very active. The debris lobes at the bottom have extended further downslope and the boulder field has expanded in the central part. On recent imagery from GoogleEarth the stabilization works are clearly visible, including various drains across the slide (E) and drainage blankets surrounding the toe of the debris lobes (F). The vegetation cover indicates that these works were successful and activity has slowed down.

DEMs and orthophotos

Automatically extracted DEMs were produced from all epochs, using a grid spacing of 1 or 2 m. The low

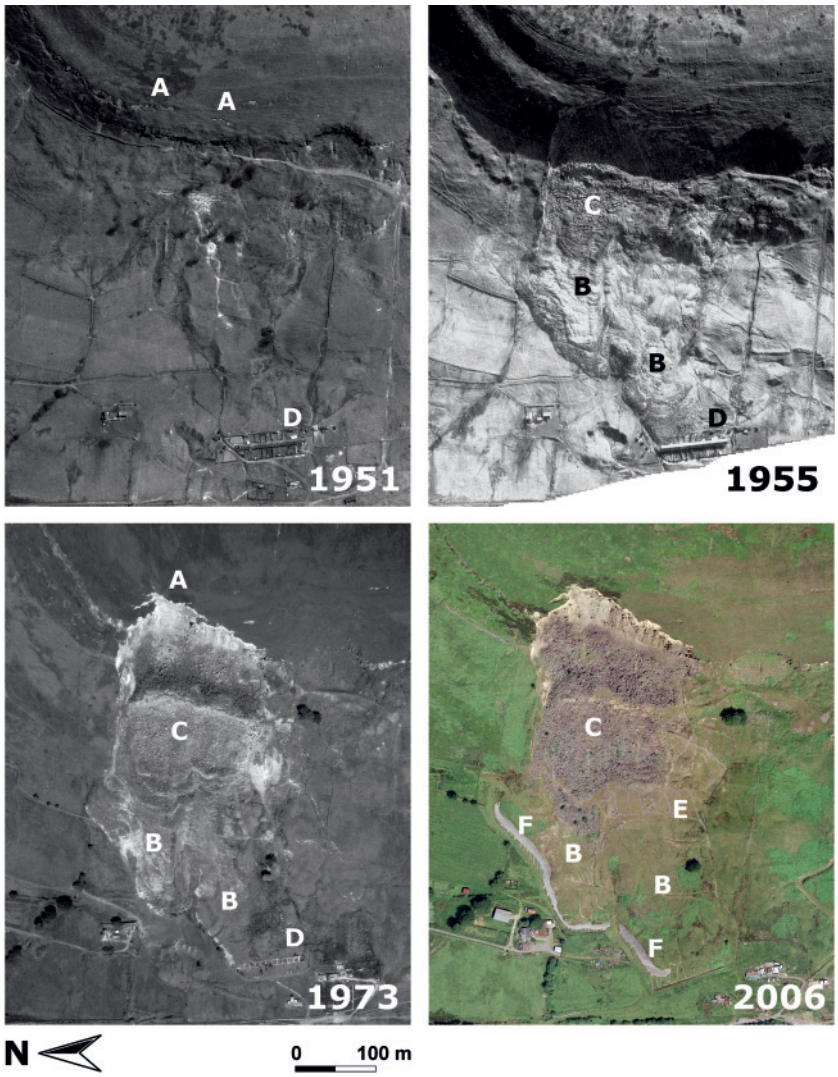

Fig. 14. An orthophoto sequence showing the stages in the development of the East Pentwyn landslide: situation just before (1951) and after (1955) the catastrophic event, continuing displacements (1973) and stabilization measures clearly visible on recent imagery (*c*. 2006; copyright reserved Google Earth). Characteristic features: A, tension fissures; B, debris lobes; C, boulder field; D, houses of Henwaun Row; E, drains; F, drainage blankets.

contrast in extensive parts of the images, especially the uphill area adjacent to the landslide, and the steep valley sides, proved to be particularly difficult for automated DEM extraction. The very low vertical accuracy of the adjustments of the 1951 and 1955 epochs resulted in equally large DEM errors (Table 4). Because of the poor DEM quality it was not feasible to create 'DEMs of difference' that could be used to detect surface elevation changes.

Visual inspection of the orthophotos showed that the poor DEM accuracies also had a significant effect on the orthophotos. Planar distortions in the uphill areas were large and resulted in deviations between the epochs.

Displacement vectors

The 1971 and 1973 epochs were specifically selected for extracting displacement vectors. On the photographs the landslide surface is not obscured by vegetation and mainly consists of large boulders that can be identified individually (Fig. 15).

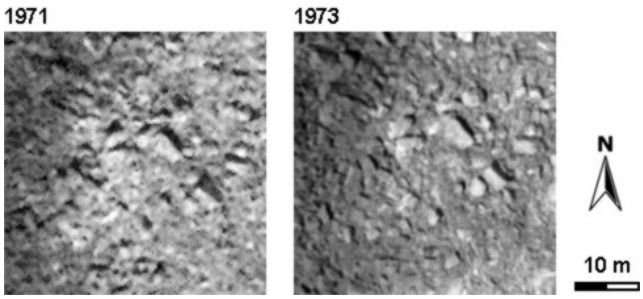

Fig. 15. Orthophotos from the 1971 and 1973 images, showing large boulders covering the East Pentwyn landslide surface.

Manual measurements of 28 points on and four points off the landslide revealed significant displacements, up to 18.5 m in horizontal direction and variable over the

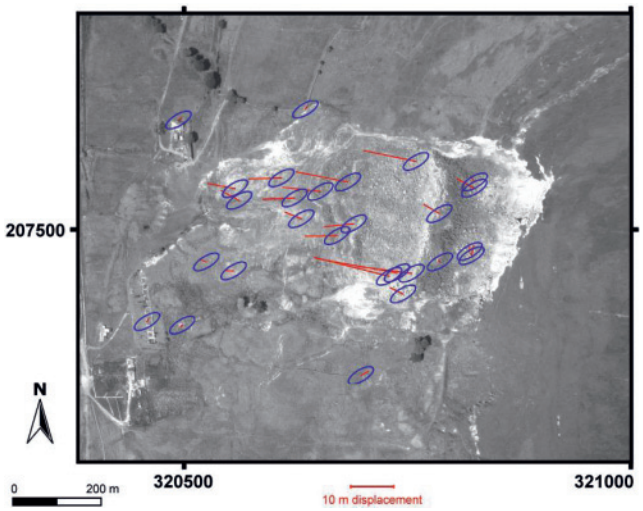

Fig. 16. Horizontal displacement vectors of the East Pentwyn landslide, obtained through measurements from the 1971 and 1973 images.

whole landslide surface (Fig. 16 and Table 5). As was also experienced in the Mam Tor study, the vertical accuracy of the data was much lower than horizontal.

The measured displacements were compared with the monitoring data provided by Halcrow (Halcrow 1983). The Halcrow data comprised repeated monitoring of movement markers located on different landslide elements. Some typical points from the datasets are compared in Table 5. Care must be taken in this comparison, as displacements are strongly temporally and spatially variable. Nevertheless, there is a striking resemblance regarding magnitude and direction of the movements. Highest rates were observed in the boulder field (almost 6 m a^{-1}) and the northern debris lobe (over 3 m a^{-1}). The movements of the displaced block and the southern debris lobe were much smaller, and in some cases insignificant.

Discussion

This study has shown that archival aerial photographs have the potential for providing a wide range of information, both qualitative and quantitative, although the quality of these data is highly dependent on the characteristics of the available imagery.

Qualitative data can be obtained through aerial photo-interpretation. Geomorphological features can be identified and mapped; their interpretation may be indicative for particular types of movement. Analysis of drainage and vegetation patterns, ground material, and geological sequences may be useful for assessing slope stability conditions. Temporal changes of these elements can be observed from image sequences and indicate the progressive development of unstable slopes. Virtually any aerial photograph with sufficient quality to distinguish surface features can be used for this type of analysis.

Photogrammetric techniques can be applied to acquire accurate quantitative data from aerial photography. Automated techniques provided by modern software packages allow high-resolution DEMs and orthophotos to be extracted easily. A DEM can be used as a source for various parameters relevant in slope stability modelling, such as slope angle, direction and length. Subtracting DEMs from different epochs is a useful tool to quantify changes of landforms; they show areas where material has been removed or deposited, and the volumes of transported material can be quantified. However, the quantitative use of DEMs may be limited by their accuracy and hence they reflect the quality of their source data. In particular, the quality of old RAF photographs was too poor for meaningful quantitative analysis. For the measurement of elevation changes it is important to consider their magnitude in relation to measurement errors. In both case histories presented in this paper, elevation changes within the terrain were too small to be detected by the DEMs with confidence. In other studies, DEM errors were of comparable size (in the range of metres) but this approach was more successful, only because the measured elevation changes were much larger (e.g. Chandler & Brunsden 1995; Baldi *et al.* 2005; Hapke 2005). Therefore, it can be concluded that this type of analysis is useful only when the displacements are relatively large (i.e. of the order of tens of metres).

A common use of orthophotographs is to provide a base-map. In this respect, they ensure that photo-interpreted information is geometrically correctly mapped and comparisons can be made between maps from different epochs. Distinct features can be identified on the landslide surface, and horizontal displacements measured. As horizontal accuracy is usually better than vertical, relatively small displacements can be measured from orthophotos. In the two case histories, significant horizontal movements could be mapped from all available photographs.

Distinct features and their displacements can also be measured directly in the stereomodels. This allows spatial and temporal displacement patterns to be analysed in three dimensions. The spatial patterns may be related to different elements within the landslide body, or used for strain analysis. Measurement of 3D displacement vectors allows estimates of shape and slope of the underlying slip surface. In some other studies, digital analysis of displacement vectors was successful, but always limited to the horizontal component (e.g. Kaufmann & Ladstädter 2002; Delacourt *et al.* 2004). Baum *et al.* (1998) measured 3D displacement vectors using analogue techniques, but found similar limitations: large displacements in horizontal directions with relatively small errors, and small vertical displacements with large errors. Oblique imagery eases this difficulty

Table 5. *East Pentwyn: comparison of photogrammetrically derived displacements with ground surveyed data (displacements are converted to yearly rates)*

Halcrow data (1982–1983)				Photogrammetric measurements (1971–1973)			
Point ID	Displacement ($m\ a^{-1}$)	Bearing (degrees)	Slope (degrees)	Point ID	Displacement ($m\ a^{-1}$)	Bearing (degrees)	Slope (degrees)
Displaced block							
15	1.98	267	9	10	2.05	300	(34)
19	1.39	268	7	9	(0.24)	(320)	(78)
Boulder field							
17	5.46	265	24	16	3.33	265	(17)
18	5.88	278	15	18	5.91	281	(14)
Debris slide (north lobe)							
8	2.99	266	14	22	3.65	268	(12)
9	3.48	276	15	24	3.16	281	(7)
Debris slide (south lobe)							
21	0.67	269	8	26	(0.84)	(290)	(32)
4	0.35	263	0	27	(0.34)	(226)	(78)

Values in parentheses are insignificant at a confidence level of 95%.

because precision is homogeneous in all three dimensions. The measurement of displacement vectors is limited to situations where the surface integrity has remained, so that features can be identified on the different images. Hence, this type of analysis is particularly useful when ground movements are relatively slow (i.e. in the range of tens of centimetres to metres), and provided that image scale and geometry allows detection.

In addition to providing a source for quantitative data, DEMs and orthophotos are essential sources for visualization. Realistic 3D views of the area from any perspective can be created, which are helpful for interpretation and presentation. Animated sequences of images provide a very useful tool for illustrating the progressive change occurring within a landslide. Data accuracy issues are less important in such analyses.

Evidently, a very important aspect of quantitative analysis is the requirement of assessing the quality of data. Input data are of primary importance for the final data accuracy. However, when using archival material, there is little control over source data quality, and the required accuracy should be considered beforehand. Primary controls are ground resolution of the images (dependent on photo-scale and scan resolution), their geometry (base distance/height ratio) and the availability of camera calibration data. When good-quality scans are available, accuracies of less than 1 m are feasible. Another limitation of historical imagery may be their radiometric quality, which will affect the performance of automated procedures for extraction of DEMs and orthophotos. In the Mam Tor case history it was demonstrated that even poor-quality scans can still provide meaningful information. The great variety of data used in the two case histories described in this paper provides a good opportunity to evaluate the controls on data quality more thoroughly. Another important development is the use of automated techniques for extracting displacement vectors from sequential images. Such techniques have been used successfully in studies on rock glaciers (Kaufmann & Ladstädter 2002), but appear less suitable for the two case histories discussed in this paper. These issues will be addressed in a future publication.

Conclusion

The two case histories have clearly demonstrated the value of the aerial photographic archive to extract spatial data necessary for assessing landslide dynamics. The locations adopted in this study were the Mam Tor and East Pentwyn landslides, both showing significant activity during the last 50 years. Archival photographs were obtained from various archives in the UK, and using an ordinary PC desktop and commercially available software useful data were extracted relatively easily. Qualitative analysis was based on aerial photo-interpretation, and appropriate photogrammetric techniques were applied for extracting quantitative data. The necessary ground control was collected using a differential GPS system.

The derived products comprised geomorphological maps, automatically derived 'DEMs of difference', displacement vectors and animations. In both case histories, the vertical component of measurements was of limited use, because of the large errors in relation to the displacements. Therefore, analysis of elevation data appears to be useful only when terrain changes are relatively large. The horizontal data proved to be more useful, and their spatial patterns could be matched with the morphological interpretation. Comparison of measured displacements with independent ground surveyed data showed good consistency.

Acknowledgements. The work described in this paper was part of collaborative research between the Geotechnical Engineering and Survey & Photogrammetry research groups in the Department of Civil and Building Engineering, Loughborough University. This research also formed the basis for J.W.'s doctoral thesis, which is available online (Walstra 2006). Special thanks are due to H. Siddle of Halcrow for providing helpful advice and useful data on the East Pentwyn landslide.

References

Adams, J.C. & Chandler, J.H. 2002. Evaluation of lidar and medium scale photogrammetry for detecting soft-cliff coastal change. *Photogrammetric Record,* **17**, 405–418.

Al-Dabbagh, T.H. & Cripps, J.C. 1987. Data sources for planning: geomorphological mapping of landslides in north-east Derbyshire. *In:* Culshaw, M.G., Bell, F.G., Cripps, I.C. & O'Hara, M. (eds) *Planning and Engineering Geology*, Engineering Geology Special Publications **4**, Geological Society, London, 101–114.

Anon 1972. The preparation of maps and plans in terms of engineering geology. Report by the Geological Society Engineering Group Working Party. *Quarterly Journal of Engineering Geology,* **5**, 297–367.

Baily, B., Collier, P., Farres, P.J., Inkpen, R. & Pearson, A. 2003. Comparative assessment of analytical and digital photogrammetric methods in the construction of DEMs of geomorphological forms. *Earth Surface Processes and Landforms,* **28**, 307–320.

Baldi, P., Fabris, M., Marsella, M. & Monticelli, R. 2005. Monitoring the morphological evolution of the Sciara del Fuoco during the 2002–2003 Stromboli eruption using multi-temporal photogrammetry. *ISPRS Journal of Photogrammetry & Remote Sensing,* **59**, 199–211.

Baum, R.L., Messerich, J. & Fleming, R.W. 1998. Surface deformation as a guide to kinematics and three-dimensional shape of slow-moving, clay-rich landslides, Honolulu, Hawaii. *Environmental & Engineering Geoscience,* **IV**, 283–306.

Boullé, P., Vrolijks, L. & Palm, E. 1997. Vulnerability reduction for sustainable urban development. *Journal of Contingencies and Crisis Management,* **5**, 179–188.

British Standards Institution 1999. *Code of practice for site investigations.* British Standards Institution, London.

Brown, D.C. 1956. *The Simultaneous Determination of the Orientation and Lens Distortion of a Photogrammetric Camera. RCA Data Reduction Technical Report 33.* ASTIA Document, **96626**.

Brunsden, D. & Prior, D.B. (eds) 1984. *Slope Instability.* Wiley, Chichester.

Brunsden, D., Doornkamp, J.C., Fookes, P.G., Jones, D.K.C. & Kelly, J.M.H. 1975. Large scale geomorphological mapping and highway engineering design. *Quarterly Journal of Engineering Geology,* **8**, 227–530.

Buckley, S.J., Mills, J.P., Clarke, P.J., Edwards, S.J., Pethick, J. & Mitchell, H.L. 2002. Synergy of GPS, photogrammetry and InSAR for coastal zone monitoring. *International Archives of Photogrammetry and Remote Sensing,* **XXXIV**, 581–586.

Carter, M. & Bentley, S.P. 1985. The geometry of slip surfaces beneath landslides: predictions from surface measurements. *Canadian Geotechnical Journal,* **22**, 234–238.

Chandler, J.H. 1999. Effective application of automated digital photogrammetry for geomorphological research. *Earth Surface Processes and Landforms,* **24**, 51–63.

Chandler, J.H. & Brunsden, D. 1995. Steady state behaviour of the Black Ven mudslide: the application of archival analytical photogrammetry to studies of landform change. *Earth Surface Processes and Landforms,* **20**, 255–275.

Chandler, J.H. & Cooper, M.A.R. 1989. The extraction of positional data from historical photographs and their application to geomorphology. *Photogrammetric Record,* **13**, 69–78.

Chandler, J.H. & Moore, R. 1989. Analytical photogrammetry: a method for monitoring slope instability. *Quarterly Journal of Engineering Geology,* **22**, 97–110.

Chandler, J.H., Lane, S.N. & Walstra, J. 2007. Quantifying landform change. *In:* Fryer, J.G., Mitchell, H. & Chandler, J.H. (eds) *Applications of 3D Measurements from Images.* Whittles, Caithness.

Clarke, J.S. & Chandler, J.H. 1992. The archival photogrammetric technique: further application and development. *Photogrammetric Record,* **14**, 241–247.

Colwell, R.N. 1960. *Manual of Photographic Interpretation.* American Society of Photogrammetry, Washington, DC.

Conway, B.W., Forster, A., Northmore, K.J. & Barclay, W.J. 1980. *South Wales Coalfield Landslip Survey: Volume 1—Text.* Institute of Geological Sciences Report, **EG 80/4**.

Cooper, M.A.R. & Cross, P.A. 1988. Statistical concepts and their application in photogrammetry and surveying. *Photogrammetric Record,* **12**, 637–663.

Crozier, M.J. 1986. *Landslides: Causes, Consequences and Environment.* Croom Helm, London.

De Graaff, L.W.S., De Jong, M.G.G., Rupke, J. & Verhofstad, J. 1987. A geomorphological mapping system at scale 1:10,000 for mountainous areas. *Zeitschrift für Geomorphologie,* **31**, 229–242.

Dehn, M., Bürger, G., Buma, J. & Gasparetto, P. 2000. Impact of climate change on slope stability using expanded downscaling. *Engineering Geology,* **55**, 193–204.

Delacourt, C., Allemand, P., Casson, B. & Vadon, H. 2004. Velocity field of the 'La Clapière' landslide measured by the correlation of aerial and QuickBird satellite images. *Geophysical Research Letters,* **31**, L15619 doi:10.1029/2004GL020193.

Dixon, N. & Brook, E. 2007. Impact of predicted climate change on landslide reactivation: case study of Mam Tor, UK. *Landslides,* **4**, 137–147.

Franklin, J.A. 1984. Slope instrumentation and monitoring. *In:* Brunsden, D. & Prior, D.B. (eds) *Slope Instability.* Wiley, Chichester, 143–169.

Fryer, J.G., Mitchell, H. & Chandler, J.H. (eds) 2007. *Applications of 3D Measurements from Images.* Whittles, Caithness.

Gili, J.A., Corominas, J. & Rius, J. 2000. Using Global Positioning System techniques in landslide monitoring. *Engineering Geology,* **55**, 167–192.

Granshaw, S.I. 1980. Bundle adjustment methods in engineering photogrammetry. *Photogrammetric Record,* **10**, 181–207.

Halcrow 1983. *East Pentwyn Landslip: First report on geotechnical investigations.* Halcrow, Cardiff.

Halcrow 1989. *East Pentwyn & Bournville landslips: monitoring report 1987–1989.* Halcrow, Cardiff.

Hapke, C.J. 2005. Estimation of regional material yield from coastal landslides based on historical digital terrain modelling. *Earth Surface Processes and Landforms,* **30**, 679–697.

Hervás, J., Barredo, J.I., Rosin, P.L., Pasuto, A., Mantovani, F. & Silvano, S. 2003. Monitoring landslides from optical remotely sensed imagery: the case

history of Tessina landslide, Italy. *Geomorphology,* **54**, 63–75.

Jones, D.B. & Siddle, H.J. 1988. Geotechnical parameters for stabilisation measures to a landslide. *In:* Bonnard, Ch. (ed.) *5th International Symposium on Landslides, 10–15 July 1988, Lausanne.* AA Balkema, Rotterdam, 193–198.

Kaufmann, V. & Ladstädter, R. 2002. Monitoring of active rock glaciers by means of digital photogrammetry. *International Archives of Photogrammetry and Remote Sensing,* **XXXIV**, 108–111.

Kenefick, J.F., Gyer, M.S. & Harp, B.F. 1972. Analytical Self-Calibration. *Photogrammetric Engineering,* **38**, 1117–1126.

Leica Geosystems 2003. *Leica Photogrammetry Suite OrthoBASE & OrthoBASE Pro User's Guide.* Leica Geosystems GIS & Mapping, LLC, Atlanta, GA.

Leick, A. 1990. *GPS Satellite Surveying.* Wiley, New York.

Luhmann, T., Robson, S., Kyle, S. & Harley, I. 2007. *Close Range Photogrammetry.* Whittles, Caithness.

Mantovani, F., Soeters, R. & Van Westen, C.J. 1996. Remote sensing techniques for landslide studies and hazard zonation in Europe. *Geomorphology,* **15**, 213–225.

Mills, J.P., Buckley, S.J., Mitchell, H.L., Clarke, P.J. & Edwards, S.J. 2005. A geomatics data integration technique for coastal change monitoring. *Earth Surface Processes and Landforms,* **30**, 651–664.

Mora, P., Baldi, P., Casula, G., Fabris, M., Ghirotti, M., Mazzini, E. & Pesci, A. 2003. Global Positioning Systems and digital photogrammetry for the monitoring of mass movements: application to the Ca' di Malta landslide (northern Apennines, Italy). *Engineering Geology,* **68**, 103–121.

Ordnance Survey, 2007. OS Net. World Wide Web Address: http://www.ordnancesurvey.co.uk/oswebsite/gps/.

Parise, M. 2003. Observation of surface features on an active landslide, and implications for understanding its history of movement. *Natural Hazards and Earth System Sciences,* **3**, 569–580.

Rib, H.T. & Liang, T. 1978. Recognition and identification. *In:* Schuster, R.L. & Krizek, R.J. (eds) *Landslides Analysis and Control.* National Academy of Sciences, Washington, DC, 34–80.

Rutter, E.H., Arkwright, J.C., Holloway, R.F. & Waghorn, D. 2003. Strains and displacements in the Mam Tor landslip, Derbyshire, England. *Journal of the Geological Society, London,* **160**, 735–744.

Schenk, A.F. 1996. Automatic generation of DEMs. *In:* Cary, T., Jensen, J. & Nyquist, M. (eds) *Digital Photogrammetry. An Addendum to the Manual of Photogrammetry.* American Society for Photogrammetry and Remote Sensing, Bethesda, MD, 247–250.

Siddle, H.J. 2000. East Pentwyn landslide, Blaina. *In:* Siddle, H.J., Bromhead, E.N. & Bassett, M.G. (eds) *Landslides and Landslide Management in South Wales.* National Museums & Galleries of Wales, Cardiff, 77–80.

Skempton, A.W., Leadbeater, A.D. & Chandler, R.J. 1989. The Mam Tor landslide, North Derbyshire. *Philosophical Transactions of the Royal Society of London, Series A,* **329**, 503–747.

Slama, C.C. 1980. *The Manual of Photogrammetry* 4th. American Society for Photogrammetry, Falls Church, VA.

Smyth, C.G. & Royle, S.A. 2000. Urban landslide hazards: incidence and causative factors in Niterói, Rio de Janeiro State, Brazil. *Applied Geography,* **20**, 95–117.

Soeters, R. & Van Westen, C.J. 1996. Slope instability recognition, analysis, and zonation. *In:* Turner, A.K. & Schuster, R.L. (eds) *Landslides. Investigation and Mitigation.* National Academy Press, Washington, DC, 129–177.

Squarzoni, C., Delacourt, C. & Allemand, P. 2003. Nine years of spatial and temporal evolution of the La Valette landslide observed by SAR interferometry. *Engineering Geology,* **68**, 53–66.

Squarzoni, C., Delacourt, C. & Allemand, P. 2005. Differential single-frequency GPS monitoring of the La Valette landslide (French Alps). *Engineering Geology,* **79**, 215–229.

Tarchi, D., Casagli, N., Fanti, R. *et al.* 2003. Landslide monitoring by using ground-based SAR interferometry: an example of application to the Tessina landslide in Italy. *Engineering Geology,* **68**, 15–30.

Uren, J. & Price, W.F. 2006. *Surveying for Engineers.* Palgrave Macmillan, Basingstoke.

Van Westen, C.J. & Getahun, F.L. 2003. Analyzing the evolution of the Tessina landslide using aerial photographs and digital elevation models. *Geomorphology,* **54**, 77–89.

Varnes, D.J. 1978. Slope movement types and processes. *In:* Schuster, R.L. & Krizek, R.J. (eds) *Landslides—Analysis and Control.* Transportation Research Board Special Report, **176**, 12–33.

Walstra, J. 2006. *Historical aerial photographs and digital photogrammetry for landslide assessment*. PhD thesis, Loughborough University. World Wide Web Address: http://hdl.handle.net/2134/2501.

Walstra, J. 2007. *Historical aerial photographs and digital photogrammetry for landslide assessment—animations*. World Wide Web Address: http://civil-unrest.lboro.ac.uk/cvjhc/jan/index.htm.

Waltham, A.C. & Dixon, N. 2000. Movement of the Mam Tor landslide, Derbyshire, UK. *Quarterly Journal of Engineering Geology and Hydrogeology,* **33**, 105–123.

Weibel, R. & Heller, M. 1991. Digital terrain modelling. *In:* Maguire, D.J., Goodchild, M.F. & Rhind, W.D. (eds) *Geographical Information Systems: Principles and Applications.* Longman, Harlow, 269–297.

Wolf, P.R. & Dewitt, B.A. 2000. *Elements of Photogrammetry. With Applications in GIS.* McGraw–Hill, Boston, MA.

Received 23 March 2007; accepted 31 July 2007.